

Thermodynamic properties of the gluon plasma

Thomas A. DeGrand

Physics Department, University of Colorado, Boulder, Colorado

Carleton E. DeTar

Physics Department, University of Utah, Salt Lake City, Utah

(Received 8 September 1986)

We calculate the energy density, pressure, and speed of sound in the deconfined phase of lattice SU(3) gauge theory at finite temperature for lattices of temporal size $N_t=4, 6, \text{ and } 8$. We compare our results with perturbative QCD at high temperature and with a simple phenomenological model. We also parametrize our results using the "bag" equation of state.

I. INTRODUCTION

There has been a great deal of interest in recent years in the properties of hadronic matter at high temperature and/or density. It is now well established that at sufficiently high temperature the SU(3) Yang-Mills gauge theory undergoes a phase transition from a confining phase into a phase in which the forces between quarks are Debye screened. At very high temperature, the major part of the statistical ensemble in QCD is well described as a gas of nearly free quarks and gluons, but at lower temperatures in the vicinity of the phase transition, the theory is very complicated. (For a discussion see Ref. 1.)

It is expected that the high energies or densities which are needed to achieve the new phase of matter may be attained in relativistic heavy-ion collisions. Relativistic hydrodynamics is the best method currently available for modeling the space-time evolution of hadronic matter during a collision. It requires as its input quantities such as the energy density, pressure, and speed of sound of hadronic matter on either side of the phase transition, a region of parameters for which perturbation theory is not applicable.

Nearly all the information which we have about QCD near the deconfinement transition comes from Monte Carlo simulation. The first computation of thermodynamic quantities for a gauge theory was done [for SU(2)] by Engels, Karsch, Montvay, and Satz.² Svetitsky and Fucito³ have computed the latent heat in pure SU(3) gauge theory. More recently, Gocksch and Gavai⁴ have calculated the energy density and speed of sound in pure SU(3) gauge theory on a lattice with the number of time steps N_t equal to 4. Following in this tradition in this paper, we calculate the energy density and pressure of pure gluonic matter on moderately large lattices and attempt to extend our results to the continuum limit. Our statistics are comparable with those of Ref. 4, while our data sample includes lattices of temporal size $N_t=4, 6, \text{ and } 8$.

We will briefly review the necessary formalism; for a detailed discussion, see Ref. 2. We then describe our data sample and our method of analysis. To anticipate our results, we see behavior in the energy density and pressure which is Stefan-Boltzmann-like at high temperature even

though the same data sample also shows correlation functions characterized by the presence of massive excitations in color-singlet channels.⁵ At the end of the paper we will describe a simple phenomenological model which describes the behavior of the energy density in terms of effective modes of the plasma.

II. EXTRACTING THERMODYNAMICS FROM LATTICE QUANTITIES

The calculation of the energy density and pressure was first given by the authors of Ref. 2. The partition function for pure gauge theory is

$$Z = \int [dU] e^{-\beta S(U)}, \tag{2.1}$$

where

$$S(U) = \sum \text{Re Tr } U_\mu(x) U_\nu(x + \hat{\mu}) U_\mu^\dagger(x + \hat{\nu}) U_\nu^\dagger(x) \tag{2.2}$$

is the Wilson action. Here β is related to the bare coupling g^2 by $\beta=6/g^2$ and N_t , the number of lattice spacings in the time direction, is related to the temperature through the lattice spacing a as $T=1/(N_t a)$. The energy density ϵ and pressure P are given by

$$\epsilon = \frac{3\beta}{a^4} \{ W_t - W_s + g^2 [C_s(W_s - W) + C_t(W_t - W)] \}, \tag{2.3}$$

$$\epsilon - 3P = \Delta. \tag{2.4}$$

The constants C_s and C_t were first calculated in perturbation theory by Karsch.⁶ The quantity Δ in Eq. (2.4) is given by

$$\Delta = -18a^{-3} \frac{\partial g^{-2}}{\partial a} (W_s + W_t - 2W). \tag{2.5}$$

W_s and W_t are the expectation values of the space-space and space-time oriented plaquettes in the finite-temperature model, while W is the plaquette on a symmetric ($T=0$) lattice. Again, one must either calculate $a \partial g^{-2} / \partial a$ using perturbation theory or from Monte Carlo renormalization-group methods. Opting for the first

choice, we have

$$a^4\Delta = 18 \left[\frac{11}{8\pi^2} + g^2 \frac{51}{64\pi^4} \right] (W_s + W_t - 2W). \quad (2.6)$$

The speed of sound is defined as

$$V_s^2 = \frac{\partial P}{\partial \epsilon} \quad (2.7)$$

or

$$V_s^2 = \frac{1}{3} \left[1 - \frac{\partial \Delta}{\partial \epsilon} \right]. \quad (2.8)$$

Gavai and Gocksch calculated V_s^2 using finite differences by computing ϵ and P as a function of T , and eliminating T between them.

III. NUMERICAL RESULTS

Our data was acquired as part of a study of correlation functions in SU(3) gauge theory near the deconfinement transition.⁵ Most of that study involved measuring the response of the lattice to an external source. However, in the analysis of our data it proved convenient to fix some parameters (in particular, the expectation value of the Wilson line) to their values in the absence of a source. Plaquette measurements from Monte Carlo simulations carried out without a source are used in the analysis reported here.

We had two separate Monte Carlo codes. One was run

on the CYBER-205 at the Supercomputer Computations Research Institute at Florida State University. The other program ran on CRAY's at the Boeing Computing Services and at the University of Illinois National Center for Supercomputer Applications. Descriptions of the programs may be found in Ref. 5. The sourceless runs consumed about 30 h of CYBER time and 20 h of CRAY time.

We ran on lattices of spatial size 11^3 or $11^2 \times 15$, with time lengths $N_t = 4, 6, \text{ and } 8$. Our data sets have from 2000 to 4000 sweeps per value of β , starting typically from lattices which had been equilibrated at a nearby value of β .

We also need the expectation values of plaquettes on symmetric ($T=0$) lattices. We did not generate those quantities as part of our simulation. Instead, we chose to work with the high-statistics plaquette expectation values of Barkai, Moriarty, and Rebbi⁷ taken on a $16^3 \times 32$ lattice. These authors present data at $\beta = 5.6, 5.8, 6.0, 6.2, \text{ and } 6.4$. We interpolated their data to our β values using a three-point interpolation. (A similar procedure was done in Ref. 2; the authors of Ref. 4 could compare against their own $T=0$ data.)

The calculation of ϵ and Δ is now straightforward. Our data were collected in a series of short computer runs and then averaged. In calculating ϵ we found it convenient to calculate the error on the quantity $W_s - W_t$ on a run-by-run basis rather than computing the error in the difference based on the errors of W_s and W_t separately. This is because fluctuations in the quantities W_s and W_t are correlated; we can actually determine their difference

TABLE I. Energy density and Δ measured in this simulation.

N_t	β	T/Λ_L	$10^{-8} \frac{\epsilon}{\Lambda_L^4}$	$10^{-8} \frac{\Delta}{\Lambda_L^4}$
4	5.72	77.8	2.40±0.13	2.88±0.06
4	5.75	80.4	2.74±0.18	2.79±0.07
4	5.77	82.3	2.96±0.13	2.72±0.05
4	5.80	85.1	3.09±0.47	2.20±0.12
4	5.90	95.2	6.41±0.77	2.90±0.18
4	5.95	100.7	6.72±0.27	2.62±0.18
4	6.00	106.6	8.10±0.22	2.22±0.18
6	5.70	50.7	0.18±0.11	0.43±0.07
6	5.75	53.6	0.13±0.13	0.37±0.06
6	5.80	56.7	0.18±0.18	0.25±0.07
6	5.83	58.7	0.33±0.19	0.65±0.09
6	5.86	60.7	0.24±0.23	0.48±0.07
6	5.90	63.5	0.63±0.20	1.21±0.10
6	5.95	67.2	0.95±0.22	1.16±0.03
6	6.00	71.0	1.51±0.38	0.95±0.14
6	6.05	75.2	2.59±1.07	1.17±0.18
6	6.11	80.4	2.01±0.67	1.48±0.27
6	6.15	84.1	3.22±2.21	0.90±0.39
6	6.20	89.0	2.88±1.39	0.91±0.66
8	5.85	45.0	0.12±0.14	0.49±0.07
8	5.95	50.4	0.08±0.25	0.50±0.10
8	6.00	53.3	0.27±0.26	0.10±0.12
8	6.05	56.4	0.66±0.28	0.58±0.10
8	6.07	58.0	0.62±0.64	0.85±0.23
8	6.15	63.1	0.47±0.19	0.71±0.19
8	6.17	64.5	1.32±0.56	0.90±0.21

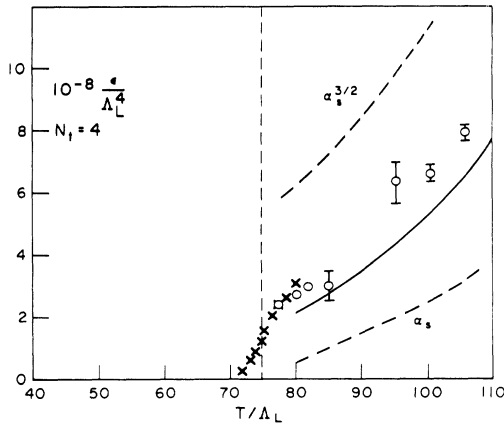


FIG. 1. The energy density ϵ/Λ_L^4 vs T/Λ_L for $N_f=4$. Crosses show the results of Ref. 4, and the vertical dashed line shows the location of the deconfinement phase transition. The smooth line is the continuum energy density for a Stefan-Boltzmann gas. The dashed lines are the predictions of perturbative QCD through $O(\alpha_s)$ and $O(\alpha_s^{3/2})$.

more accurately than we can determine their individual values. Our results are presented in Table I. For further analysis, we will break our data down into subsamples and deal with each of the subsamples separately.

Our data for $N_f=4$ are shown in Figs. 1 and 2, along with the results of Ref. 4. Their ϵ data and ours appear to lie along a smooth curve which rises with T/Λ_L . Our data for Δ disagree with the data of Ref. 4 where they overlap with it, but we cannot quantify this disagreement since they do not quote errors. At higher T/Λ_L our data show that the parameter Δ appears to level off.

Much of the analysis of Sec. II involves taking the continuum limit using the perturbative β function. Unfortunately, perturbation theory is not believed to be applicable for $\beta \lesssim 6.0$. For example, asymptotic scaling in

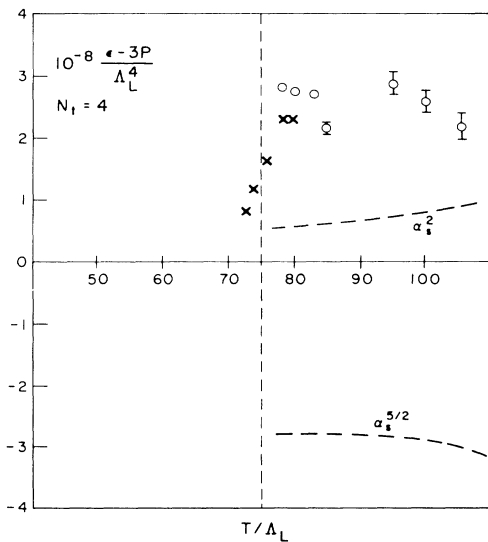


FIG. 2. The parameter Δ/Λ_L^4 vs T/Λ_L for $N_f=4$. The labels are the same as for Fig. 1. The curves show the QCD perturbation theory for the parameter Δ through $O(\alpha_s^2)$ and $O(\alpha_s^{5/2})$.

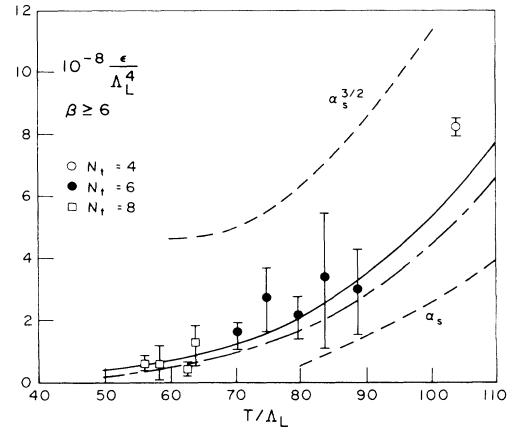


FIG. 3. The energy density ϵ/Λ_L^4 for $\beta \geq 6.0$ vs T/Λ_L . Open circles, solid circles, and boxes label $N_f=4$, 6, and 8, respectively. The smooth line is the continuum energy density for a Stefan-Boltzmann gas. The dashed lines are as in Fig. 1, and the long- and short-dashed line shows the prediction of the effective model described in Sec. IV B.

agreement with the two-loop perturbative β function for the deconfinement transition temperature is known to set in only at β greater than about 6.1 (Refs. 8 and 9). In an attempt to remove gross scaling violations, we plot in Figs. 3 and 4 all of our data for which $\beta \geq 6.0$. The data show a rapid increase in the energy density with temperature.

For comparison, we superpose on Figs. 1 and 3 the expected energy density from a continuum gas of eight massless noninteracting vector bosons. Remarkably, the data all lie on the curves, confirming previous observations.^{2,10} We have attempted to verify this behavior by fitting the energy density to the form

$$\epsilon = A + B \frac{\pi^2}{15} T^4, \quad (3.1)$$

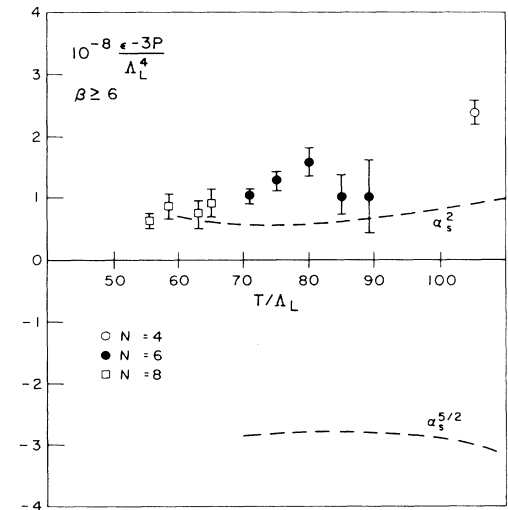


FIG. 4. The quantity Δ/Λ_L^4 for $\beta \geq 6.0$ vs T/Λ_L . Open circles, solid circles, and boxes label $N_f=4$, 6, and 8, respectively. The curves are as in Fig. 2.

TABLE II. Fits to the energy density.

Data	Number of points	A	B	σ^2
$N_t=4$	7	$0.12 + 0.1 - 0.15$	9.8 ± 1.0	3.3
$N_t=4, 6, 8$	10	-0.32 ± 0.15	9.7 ± 0.3	4.9
$N_t=6, 8$	9	-0.10 ± 0.15	8.15 ± 2.5	4.4

where B counts the effective number of massless vector degrees of freedom. Results of this fitting procedure are shown in Table II for selected subsets of the data. Our $N_t=4$ data are fit by $B=9.8 \pm 1.0$. Our $\beta \geq 6$, $N_t=6, 8$ data give $B=8.2 \pm 2.5$.

Our data are too noisy to extract a speed of sound for the plasma using the numerical derivative method of Ref. 4. The most we can say is that the parameter Δ does not show any striking rise with temperature, unlike ϵ . For example, in Fig. 4 Δ is constant as the temperature varies. This result suggests that the speed of sound is approximately $(\frac{1}{3})^{1/2}$ for T/Λ_L greater than about 50. We remark that our data show too much fluctuation for us to give a reliable value for the latent heat.

We conclude this section with some warnings about our numerical analysis. The analysis of the pressure and energy density is much more model dependent than the analysis of other quantities on the lattice.

(1) There are delicate cancellations between the $T=0$ and $T \neq 0$ plaquette values. Our plaquette values have errors in the fifth decimal place, which can result in a 30–50% error in the energy density. There may be unknown systematic errors in comparing our plaquette values with those of Ref. 7.

(2) Many quantities in the analysis have been calculated using perturbation theory, yet the data are mainly taken in a range of β 's for which asymptotic scaling is known not to work.

IV. DISCUSSION

We will conclude this paper by comparing our Monte Carlo results with the predictions of two models.

A. Perturbation theory

Our first model for the behavior of ϵ and Δ is perturbation theory. Kapusta¹¹ has computed the thermodynamic potential Ω to $O(g^3)$. Thermodynamics tells us that if

$$\Omega = -VT^4 f(T), \quad (4.1)$$

then

$$\Delta = T^4 \left[T \frac{\partial f}{\partial T} \right] \quad (4.2)$$

and

$$\epsilon = 3T^4 f + \Delta. \quad (4.3)$$

Differentiating Kapusta's expression for Ω we find

$$\frac{\epsilon}{\Lambda_L^4} = \left[\frac{T}{\Lambda_L} \right]^4 \left[\frac{8\pi^2}{15} - 8\pi\alpha_s + 128\sqrt{\pi}\alpha_s^{3/2} \right] \quad (4.4)$$

and

$$\frac{\Delta}{\Lambda_L^4} = \left[\frac{T}{\Lambda_L} \right]^4 \frac{22\alpha_s^2}{\pi} \left[\frac{8\pi}{3} - 64\sqrt{\pi}\alpha_s \right]. \quad (4.5)$$

The running coupling constant is

$$\alpha_s(T) = \frac{\pi}{12} \left[\frac{11}{6} \ln \left[\frac{T}{\kappa\Lambda_L} \right] + \frac{17}{22} \ln \ln \left[\frac{T}{\kappa\Lambda_L} \right] \right]^{-1} \quad (4.6)$$

with $\kappa=31.3$ to convert from lattice regularization to the Pauli-Villars regularization of Ref. 11.

At low values of T/Λ_L perturbation theory is poorly behaved. At $T/\Lambda_L=80$ the $O(\alpha_s)$ correction to ϵ is $\frac{3}{4}$ as big as the Stefan-Boltzmann term, and the $O(\alpha_s^{3/2})$ term is 2 times as big as the Stefan-Boltzmann term. The $O(\alpha_s^{3/2})$ term remains larger than the Stefan-Boltzmann term for $T/\Lambda_L \leq 120$. For this reason the much-celebrated finding that the leading-order perturbative contribution, i.e. the Stefan-Boltzmann formula, agrees with the data can scarcely be taken as a confirmation of the idea that the plasma is a weakly interacting gas at these temperatures. We plot the $O(\alpha_s)$ and $O(\alpha_s^{3/2})$ contributions to Eq. (4.4) in Figs. 1 and 3. It should be noted that some finite-size effects studied in Ref. 2 would decrease the measurements by about 30%. However, our pessimistic conclusions are unchanged.

For all values of T/Λ_L appropriate to our simulation the $\alpha_s^{5/2}$ term in Δ is bigger than the α_s^2 term, and it drives Δ negative. This poor convergence property of the thermodynamic potential is well known. We compare our data with the $O(\alpha_s^2)$ and $O(\alpha_s^{5/2})$ calculations in Figs. 2 and 4.

B. Three-component model

Our second phenomenological model is based on the picture of the plasma given in Ref. 1. In the plasma there are at least three important length scales. First, in order of magnitude, there is the Debye screening scale

$$m_D \simeq gT \equiv \mu_D T, \quad (4.7)$$

and second, the scale for magnetic confinement

$$m_M \simeq g^2 T \equiv \mu_M T. \quad (4.8)$$

In these formulas $g(T)$ is the temperature-dependent coupling constant; $g^2(T) = 16\pi\alpha_s(T)$ and the running coupling constant α_s is given by Eq. (4.6). Third, there is an inverse mean free path m_{MF} which marks the upper momentum cutoff for the plasma to support collective hydrodynamic fluctuations. The inverse mean free path for gluons has been calculated in perturbation theory by Shuryak¹² to be

$$m_{MF} \simeq 30\alpha_s^2(T)T \equiv \mu_{MF} T. \quad (4.9)$$

Since this distance is shorter than the magnetic confinement scale, the mean free path relevant to hydrodynamics should be calculated instead for the color-singlet modes. We offer a different estimate below.

For distances much shorter than $1/m_D$ or $1/m_M$ the plasma is economically described as a gas of noninteracting gluons. For distances longer than or on the order of

$1/m_M$ or $1/m_D$, confining effects are important. For distances much longer than $1/m_{MF}$, hydrodynamic modes are important. Thus we suggest a crude three-component model of the plasma as a gas of free high-momentum gluons, low-momentum noninteracting color-singlet modes, and low-momentum hydrodynamic phonons.¹³ This model is somewhat reminiscent of the Landau theory of liquid ^4He (Ref. 14). Clearly there is some risk of multiple counting of degrees of freedom, since the color-singlet excitations and the phonons are collective excitations of gluons. However, there is some consolation in the observation that the effect of excluding low-momentum color-octet gluons and replacing them by a few color-singlet modes is to reduce the number of degrees of freedom compared with a pure Stefan-Boltzmann gas of gluons.

We calculate the energy density by breaking momentum space into a sequence of regions and keeping only the most important contribution in each region. For $k > m_D$ those degrees of freedom are eight noninteracting massless gluons. For $k < m_M$ they are the magnetically confined color-singlet modes. For $k < m_{MF}$ the phonon also contributes to the energy density.

Because all the scales in Eqs. (4.7)–(4.9) vary linearly with the temperature (up to logarithmic corrections) each of the regions of momentum space gives a contribution to the energy density which is proportional to T^4 . Expressed in units of the contribution of a single spinless, massless boson, the internal energy of the plasma is

$$\epsilon = \frac{\pi^2 T^4}{30} u, \quad (4.10)$$

where

$$u = u_{\text{ph}}(\mu_{\text{MF}}) + u_M(\mu_M) + u_E(\mu_D) + 16u_G(\mu_D), \quad (4.11)$$

where the phonon contribution is

$$u_{\text{ph}}(\mu) = \frac{15}{\pi^4} \int_0^\mu \frac{p^2 dp V_{sP}}{e^{V_{sP}} - 1}. \quad (4.12)$$

The terms u_M and u_E weight the color-singlet modes: per magnetic mode,

$$u_M(\mu) = \frac{15}{\pi^4} \int_0^\mu \frac{p^2 dp (p^2 + \mu^2)^{1/2}}{\exp[(p^2 + \mu^2)^{1/2}] - 1} \quad (4.13)$$

[the formula for $u_E(\mu)$ is identical] and u_G the gluon modes

$$u_G(\mu) = \frac{15}{\pi^4} \int_\mu^\infty \frac{p^3 dp}{e^p - 1}. \quad (4.14)$$

In the spirit of this model, we can now estimate the inverse mean free path. It is governed by the size and density of the color-singlet modes, since they control the longest-range interactions. Their size is set by the confinement scale $1/m_M$ and since they exist only for momenta smaller than m_M , their density, given by the Boltzmann distribution, is of order m_M^3 . Thus, the mean free path is of order

$$m_{\text{MF}} \simeq m_M. \quad (4.15)$$

We infer from previous work⁵ that μ_D (and probably μ_M) range between 1 and 3 for the temperature range of interest. We also know that m_{MF} is no bigger than $\mu_D T$. Taking $V_s = (\frac{1}{3})^{1/2}$ we can numerically evaluate the integrals of Eqs. (4.12)–(4.14) for this range of μ . The results are shown in Fig. 5. As the parameter μ rises (as the temperature falls) the phonons take a larger share of the energy density. The massive confined modes never contribute more than 10% of a single massless boson mode. Only for very large μ does the energy deviate appreciably from the free gluon result.

In Ref. 5 we found that μ_D could be fit by the simple functional form

$$\mu_D \simeq 0.79g(T). \quad (4.16)$$

Thus as T/Λ_L rises from 60 to 100, μ_D falls from a value of about 3 to about 2. Including this variation of μ_D with T but keeping the breakup in momentum space exactly as in Eqs. (4.12)–(4.14), taking μ_D , μ_M , and μ_{MF} all equal, and counting one magnetic and one electric mode in ϵ , we get the long and short dashed curve shown in Fig. 3. It is entirely consistent with our $N_t = 6$ and 8 data but considerably undershoots our $N_t = 4$ points.

This simple model is much too crude to apply to the quantity Δ . This term measures the interaction strength of the plasma, yet the model assumes that the various modes of the plasma do not interact. The quantity Δ is also very sensitive to the details of the model. For example, if we chose to make the momentum-space cutoffs in the thermodynamic potential instead of the energy density, and if we took the coefficients μ to be temperature independent, we would find that $\Delta = 0$. More detailed modeling clearly lies outside the scope of this paper.

C. “Bag” equation of state

Most hydrodynamic calculations of the plasma use the “bag” equation of state¹⁵ for the deconfined phase of QCD:

$$\begin{aligned} \epsilon &= gT^4 + B, \\ P &= \frac{1}{3}gT^4 - B, \end{aligned} \quad (4.17)$$

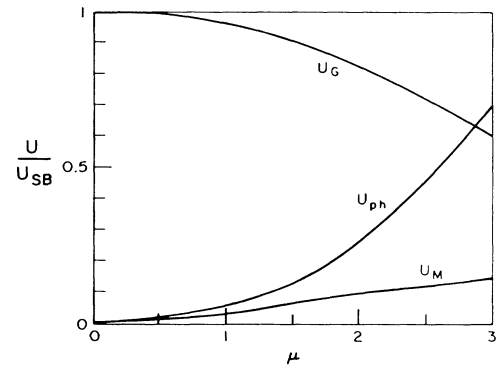


FIG. 5. Behavior of the phonon, gluon, and confined mode contributions to the energy density of the plasma as a function of the cutoff parameter μ . The modes are shown as a fraction of a massless boson's contribution to the energy density.

where B is a constant. In the bag equation of state, the latent heat L is equal to $4B$. Figures 3 and 4 suggest that this equation of state can reproduce the gross features of the deconfined phase. Comparing our data with this equation of state, we have g appropriate to eight massless vector gluons and [using the results of Refs. 8 and 9 to give the ratio (T_c/Λ_L)], $4B \simeq 13.2T_c^4$.

V. CONCLUSIONS

Within the limitations of our rendering of the Monte Carlo simulation, we find that although the energy density of the pure gluon plasma appears to follow a Stefan-Boltzmann curve at temperatures above but near the phase transition, this behavior is inconsistent with the next two leading terms in perturbative QCD, and so cannot justify the hypothesis that the plasma consists of a nearly free gas of gluons at these temperatures. We have formulated a crude model designed to take into account

nonperturbative effects by characterizing the plasma as a gas of three noninteracting components: high-momentum gluons and low-momentum color-singlet modes and photons, and find that it can account for the measurements; however, it is not known how interactions in this model would alter this agreement. In the interest of reconciling the two approaches, it would be worthwhile repeating the perturbative calculations of the gluon contribution to the thermodynamic potential using a low-momentum cutoff in the gluon propagator to see whether convergence is thereby improved. More lengthy simulations with smaller errors would also be welcome.

ACKNOWLEDGMENTS

This work was supported by the U.S. Department of Energy (T.D.) and by the National Science Foundation (C.D.). One of us (T.D.) would like to thank Keijo Kajantie and Ben Svetitsky for discussions.

¹C. DeTar, Phys. Rev. D **32**, 276 (1985).

²J. Engels, F. Karsch, I. Montvay, and H. Satz, Nucl. Phys. **B205**, 545 (1982); Phys. Lett. **101B**, 89 (1981).

³B. Svetitsky and F. Fucito, Phys. Lett. **131B**, 165 (1983).

⁴A. Gocksch and R. Gavai, Phys. Rev. D **33**, 614 (1986).

⁵T. DeGrand and C. DeTar, Phys. Rev. D **34**, 2469 (1986).

⁶F. Karsch, Nucl. Phys. **B205**, 285 (1982).

⁷D. Barkai, K. Moriarty, and C. Rebbi, Phys. Rev. D **33**, 2201 (1984).

⁸S. Gottlieb, J. Kuti, D. Toussaint, S. Meyer, B. Pendleton, and R. Sugar, Phys. Rev. Lett. **55**, 1958 (1985).

⁹N. Christ and A. Terrano, Phys. Rev. Lett. **56**, 111 (1986).

¹⁰I. Montvay and E. Pietarinen, Phys. Lett. **110B**, 148 (1982); **115B**, 151 (1982).

¹¹J. Kapusta, Nucl. Phys. **B148**, 461 (1979).

¹²E. Shuryak, Phys. Rep. **61**, 71 (1981).

¹³P. Carruthers, Phys. Rev. Lett. **50**, 1179 (1983).

¹⁴See W. Yourgraw, A. van der Merwe, and G. Raw, *A Treatise on Irreversible and Statistical Thermodynamics* (McMillan, New York, 1966).

¹⁵K. Kajantie, R. Ratio, and V. Ruuskanen, Nucl. Phys. **B222**, 152 (1983).